Journal of
Synchrotron
Radiation

ISSN 0909-0495

Received 9 November 2010
Accepted 16 February 2011

In situ powder diffraction study of belite sulfoaluminate clinkering

Ángeles G. De la Torre, Antonio J. M. Cuberos, Gema Álvarez-Pinazo, Ana Cuesta and Miguel A. G. Aranda*

Departamento de Química Inorgánica, Cristalografía y Mineralogía, University of Malaga, 29071 Malaga, Spain. E-mail: g_aranda@uma.es

Belite sulfoaluminate (BSA) cements have been proposed as environmentally friendly building materials, as their production may release up to 35% less CO_2 into the atmosphere when compared with ordinary Portland cement fabrication. However, their formation mechanism has not been studied in detail so far. Here, an *in situ* high-temperature high-resolution synchrotron X-ray powder diffraction study is reported. Two types of BSA clinkers have been characterized, both containing 50–60 wt% C_2S and 20–30 wt% $C_4A_3\underline{S}$ as main phases. One type is iron-rich and a second type (with different phase assemblage) is aluminium-rich. Furthermore, the C_2S phase reacts slowly with water, thus activation of this compound is desirable in order to enhance the mechanical strength development of the resulting cements. To do so, iron-rich BSA clinkers have been doped with minor amounts of B_2O_3 and Na_2O to promote stabilization of α-forms of C_2S, which are more reactive with water. The decarbonated raw materials were loaded into Pt tubes and heated to between 973 K and 1673 K, and patterns were collected using a high-energy synchrotron beam of wavelength λ = 0.30 Å. The thermal stability of Klein's salt in these clinkers has been clarified. Several reactions have been followed: formation and decomposition of Klein's salt, melting of aluminates and ferrite, and polymorphic transformations of dicalcium silicate: α'_H-$C_2S \rightarrow \alpha$-C_2S. Changes in mineralogical phase assemblages at a given temperature owing to the addition of minor amounts of selected elements have also been determined.

Keywords: quantitative phase analysis; Rietveld method; high-temperature X-ray powder diffraction; clinkering; belite sulfoaluminate.

1. Introduction

In recent years belite sulfoaluminate (BSA) cement research has increased (Gartner, 2004; Phair, 2006) as a consequence of some intrinsic advantages. These materials consume less energy during manufacturing when compared with ordinary Portland cement (OPC) production (Arjunan *et al.*, 1999; Beretka *et al.*, 1996; Janotka *et al.*, 2007; Quillin, 2001). BSA clinker formation requires lower temperatures in the kiln and they are easier to grind. Moreover, the elemental dosage of BSA cement demands less calcium and more sulfate than OPC, and consequently less calcium carbonate is included in the raw meals (Glasser & Zhang, 2001). Taking into account these facts, CO_2 emissions may be depleted up to 35%, comparing with OPC production. BSA cements also contribute to reduce the use of natural resources by allowing the use of a variety of industrial waste materials (Arjunan *et al.*, 1999; Selcuk *et al.*, 2010; Adolfsson *et al.*, 2007). Moreover, the lower kiln temperature depletes NO_x emissions during manufacturing of BSA cements (Quillin, 2001).

Hereafter, cement nomenclature will be used: C = CaO, S = SiO_2, A = Al_2O_3, F = Fe_2O_3, $\underline{S}$ = SO_3 and H = H_2O. The most common formulations of BSA cements are C_2S, $C_4A_3\underline{S}$ and C_4AF (Glasser & Zhang, 2001; Quillin, 2001; Adolfsson *et al.*, 2007; Janotka *et al.*, 2007). These are iron-rich BSA cements produced at ~1520 K and they are characterized by rapid hardening, high resistance to sulfate attack, self-stressing and volume stability, depending on the amount of gypsum added (Pera & Ambroise, 2004; Winnefeld & Barlag, 2009). BSA cements can be classified as belite-rich materials when containing more than 50 wt% C_2S, while OPCs are alite-rich cements with more than 60 wt% C_3S (Taylor, 1997). However, the massive application of these materials requires overcoming at least one main drawback: the low hydration rate of the belite phase, which leads to low strength development at early hydration ages (Popescu *et al.*, 2003). To overcome this technological problem the stabilization of high-temperature belite polymorphs (α-forms) is considered the best alternative, as they react with water at a higher pace than the β-form (Li *et al.*, 2001; Li & Gartner, 2006; Morsli *et al.*, 2007*a*,*b*; Cuberos *et*

al., 2010). Whatever the formulation proposed, some questions about the clinker formation process remain open; for instance, the avoidance of the formation of some non-hydraulic phases such as C_2AS or $C_5S_2\underline{S}$ (Arjunan *et al.*, 1999; Li *et al.*, 2001) at the expense of $C_4A_3\underline{S}$.

It must be highlighted that high-resolution monochromatic synchrotron X-ray powder diffraction (SXRPD) has been previously employed for quantitative phase analysis of anhydrous cements at room temperature (De la Torre & Aranda, 2003; Peterson *et al.*, 2006), and to follow hydration reactions (Christensen *et al.*, 2003; Merlini *et al.*, 2008; Cuberos *et al.*, 2009). Furthermore, clinkering is a complex set of processes as it comprises high-temperature solid-state reactions, liquid phase appearance (melting), polymorphic transformations on heating, and polymorphic stabilization and crystallization on cooling. Main reactions/processes take place between 1300 and 1800 K. The use of high-resolution SXRPD is highly desirable for studying chemical reactions with temperature (Chung *et al.*, 1993; Gualtieri *et al.*, 2008). Using highly energetic X-rays minimizes the absorption, which allows the use of Pt capillaries to perform high-temperature *in situ* studies (Moussa *et al.*, 2003). Transmission geometry (rotating capillary) leads to the illumination of the full sample avoiding poor particle statistics that is key when the liquid phase appears. Moreover, high resolution is very important for overcoming the problem of strong peak overlapping in the patterns (De la Torre *et al.*, 2001). There are few works reporting high-temperature SXRPD *in situ* studies of cements using high-energy SXRPD (Marchi *et al.*, 2007; De la Torre *et al.*, 2007).

The main objective of this work is to study the mechanism(s) of clinkering of BSA raw materials with different mineralogical compositions. The merit of this approach is to combine high-temperature synchrotron X-ray powder diffraction data and the Rietveld method to yield accurate phase analyses as a function of temperature. Different clinkering reactions and processes are reported and discussed.

2. Experimental section

2.1. Sample preparation

2.1.1. Iron-rich clinker raw material. Kaolin (Aldrich), γ-Al_2O_3 (99.997% AlfaAesar), calcite (99.95–100.05% AlfaAesar), iron oxide (99.95% AlfaAesar) and pure gypsum were mixed to obtain iron-rich BSA clinkers with theoretical mineralogical composition: 50 wt% C_2S, 30 wt% $C_4A_3\underline{S}$ and 20 wt% C_4AF. In order to promote stabilization of α-forms of C_2S, 1.0 wt% and 2.0 wt% B_2O_3 were added to raw materials as $Na_2B_4O_7{\cdot}10H_2O$. Hereafter, these clinkers are labelled as Fe_BSA_B*x*, where *x* stands for the amount of B_2O_3 added. Table 1 gives the elemental composition of these raw mixtures.

2.1.2. Al-rich BSA raw mixture. Kaolin (Aldrich), γ-Al_2O_3 (99.997%, AlfaAesar), calcite (99.95–100.05%, AlfaAesar) and pure gypsum were mixed in order to obtain an aluminium-rich BSA clinker, hereafter called Al_BSA, with theoretical mineralogical composition: 50 wt% C_2S, 30 wt% $C_4A_3\underline{S}$, 10 wt% CA and 10 wt% $C_{12}A_7$. The nominal dosage, expressed as oxide, is also given in Table 1.

Table 1
Dosages used to obtain BSA clinkers, expressed as oxide in wt%.

	CaO	SiO_2	Al_2O_3	Fe_2O_3	SO_3	Na_2O	B_2O_3
Fe_BSA_B0	52.7	17.5	19.2	6.6	4.0	0.0	0.0
Fe_BSA_B1	52.0	17.2	18.9	6.5	3.9	0.5	1.0
Fe_BSA_B2	51.3	17.0	18.6	6.4	3.8	0.9	2.0
Al_BSA	52.0	17.4	26.6	–	3.9	–	–

All raw mixtures were preheated at 1223 K for 1 h in open Pt crucibles, in order to achieve decarbonation. These preheated (decarbonated) mixtures were introduced, in house, into Pt (99.95%) capillaries from Goodfellow with an internal free diameter of 0.57 mm and a wall size of 40 µm.

2.2. High-temperature synchrotron X-ray powder diffraction data acquisition and analysis

SXRPD patterns were collected on ID31 beamline (ESRF, Grenoble, France) in Debye–Scherrer (transmission) configuration. A short wavelength, λ = 0.29980 (3) Å (41.34 keV), was selected with a double-crystal Si (111) monochromator and calibrated with Si NIST standard (a = 5.431195 Å). The Pt capillaries were rotated at ~1000 r.p.m. during data collection to improve particle statistics. The data acquisition time was ~45 min at each temperature to assure good counting statistics over the angular range 1–20° 2θ. The multi-analyser Si(111) stage coupled with nine point detectors was used. However, only seven of them were used to normalize data owing to problems with the side detectors at such high energy. Data were summed up to 0.003° step size with local software to produce the final raw data. A parabolic mirror furnace composed of three halogen lamps (Moussa *et al.*, 2003) was used to heat the samples up to ~1700 K.

X-ray powder diffraction patterns were analysed by using the Rietveld method as implemented in the *GSAS* software package (Larson & Von Dreele, 1994) using the *EXPGUI* graphic interface (Toby, 2001), in order to obtain Rietveld quantitative phase analysis (RQPA) (Madsen *et al.*, 2001; Scarlett *et al.*, 2002). Peak shapes were fitted by using the pseudo-Voigt function (Thompson *et al.*, 1987) with the axial divergence correction implemented (Finger *et al.*, 1994). The refinement strategy for clinkers was that reported by León-Reina *et al.* (2009), by refining background coefficients, cell parameters, zero-shift error, peak shape parameters and phase fractions. RQPA were computed for the 3 to 11.7° 2θ range and the two regions where the Pt peaks gave significant contribution were excluded from the fits.

2.3. DTA-TG experimental

Differential thermal analyses and thermal gravimetry (DTA-TG) analyses were performed for raw mixtures on an SDT-Q600 analyzer from TA Instruments. The temperature was varied from room temperature up to 1723 K at a heating/cooling rate of 10 K min^{-1}. Measurements were carried out on samples in open platinum crucibles under a flow of air.

3. Results and discussion

3.1. Verification of temperature determination

The (variable) voltage applied to the halogen lamps coarsely controlled the target temperature. Furthermore, ageing of the lamps led to different temperatures for the same values of the applied voltage. Therefore, the temperatures given in this study were determined from the Pt diffraction peak positions by comparing the obtained unit-cell values with the reported platinum unit-cell thermal expansion (Arblaster, 2006). Fig. 1 shows raw data from 1° to 20° 2θ of Fe_BSA_B1 at 1423 K with Pt peaks labelled. The inset shows a selected range of the Rietveld plot where main peaks of clinker phases appear, *i.e.* 3.8° to 7.2° 2θ. However, it is very important to verify that the final reported temperatures are correct. An independent test has been carried out using the unit-cell values of the simplest best-known phase: CaO. Fig. 2 shows CaO unit-cell values as a function of the temperature for all the samples. It must be highlighted that volume modification of this phase is mainly due to the temperature variation since it does not accept a significant amount of dopants. All data are linearly arranged which confirms that the temperatures for all the patterns have been properly determined. Furthermore, the volumetric lattice thermal expansion coefficient for CaO, derived from Fig. 2, was $\alpha_v = 48.3\ (1) \times 10^{-6}\ K^{-1}$ [α_v is defined as b/a for the $V(T) = a + bT$ fit]. Under the isotropic thermal expansion approximation the linear expansion coefficient, β_{calc}, can be derived as $\beta_{calc} = \alpha_v/3 = 16.1 \times 10^{-6}\ K^{-1}$. This value is in relatively good agreement with our previous obtained coefficient, $14.5 \times 10^{-6}\ K^{-1}$ (De la Torre *et al.*, 2007), and that reported for pure CaO, $15.2 \times 10^{-6}\ K^{-1}$ (Fiquet *et al.*, 1999), both obtained from variable-temperature synchrotron X-ray powder diffraction data. These three values are, as expected, slightly larger than the bulk linear expansion of CaO, $13.6 \times 10^{-6}\ K^{-1}$ (Grain & Campbell, 1962), determined from a dilatometric study, mainly owing to the residual porosity in the ceramic body that decreases the measured value.

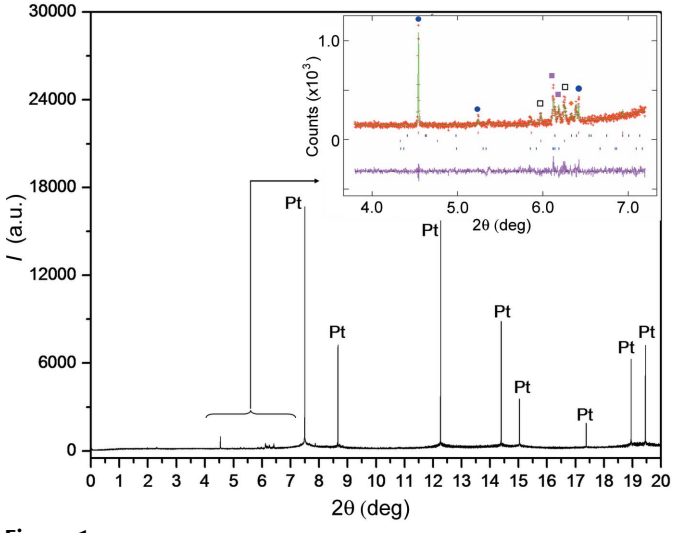

Figure 1
SXRPD raw data for Fe_BSA_B1 at 1423 K (1° to 20° 2θ) measured using $\lambda = 0.3$ Å. The sample is inside a Pt capillary and heated with halogen lamps. Inset: selected range of the Rietveld plot where main diffraction peaks of clinker phases appear. Blue circles: $C_4A_3\underline{S}$; purple squares: α'_H-C_2S; red diamond: C_4AF; open squares: α-C_2S.

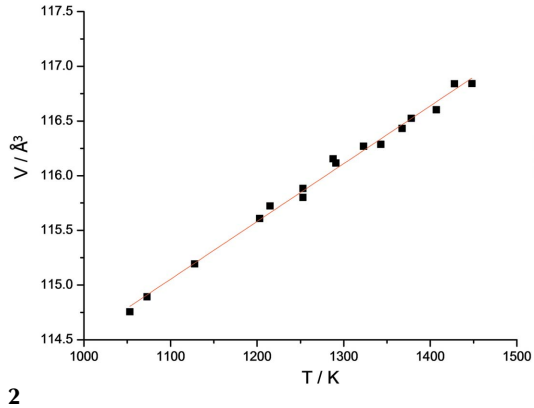

Figure 2
CaO unit-cell volume *versus* temperature from all the Rietveld refinements.

3.2. *In situ* Fe_BSA_B*x* clinker formation

RQPA has been performed for all compositions and selected temperatures. Direct RQPA results for the three compositions studied in this system are reported in Tables 2–4. Fig. 3 shows a selected range of the raw data for Fe_BSA_B1 at various temperatures, as a representative example. The diffraction peaks, arising from different phases, are labelled in order to highlight the transformations that are taking place on heating. Fig. 4 shows an enlarged range of Rietveld plots (5.9–6.5°) to show the quality of the fits. Fig. 4(*a*) displays a sample where α'_H-C_2S (purple squares) coexists with free lime (red star), $C_4A_3\underline{S}$ (blue circle) and C_4AF (red diamonds), Fe_BSA_B0 at 1428 K. On the other hand, Fig. 4(*b*) shows Fe_BSA_B1 at 1553 K where α'_H-C_2S (purple squares) coexists with α-C_2S (open squares) and $C_4A_3\underline{S}$ (blue circle). On average, the maximum intensities of the diffraction peaks of Pt were close to 30000 counts s^{-1} and the maximum intensities of

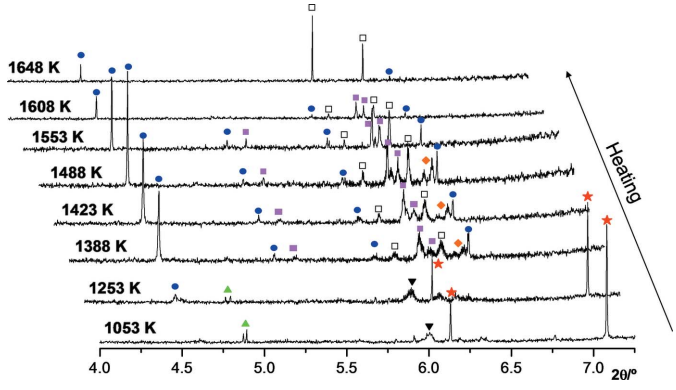

Figure 3
Three-dimensional view of a selected range of the SXRPD raw patterns for Fe_BSA_B1 clinker formation collected on heating from 1053 K to 1648 K, where the symbols highlight CaO (red stars), β-SiO_2 (black triangles), $CaSO_4$ (green triangles), $C_4A_3\underline{S}$ (blue circles), α'_H-C_2S (purple squares), C_4AF (red diamonds) and α-C_2S (open squares).

Table 2
Direct Rietveld quantitative phase analysis results (wt%) for Fe_BSA_B0 as a function of temperature (only crystalline fractions are included).

T (K)	C	β-S	C$\underline{S}$	α-C_2S	α'_H-C_2S	$C_4A_3\underline{S}$	C_4AF	C_3A
1343	19.9 (2)	24.0 (5)	3.1 (3)	–	40.2 (6)	12.8 (3)	–	–
1378	3.9 (1)	4.0 (6)	–	–	57.0 (4)	22.2 (3)	12.8 (5)	–
1428	2.1 (1)	2.6 (3)	–	–	61.1 (3)	21.6 (3)	12.6 (5)	–
1483	–	–	–	–	58.5 (4)	21.9 (3)	17.4 (6)	2.2 (3)
1543	–	–	–	–	57.5 (3)	18.8 (3)	23.7 (4)	–
1583	–	–	–	–	76.9 (2)	15.3 (3)	7.8 (4)	–
1633	–	–	–	–	90.6 (2)	9.4 (5)	–	–
1698	–	–	–	100 (–)	–	–	–	–

Table 3
Direct Rietveld quantitative phase analysis results (wt%) for Fe_BSA_B1 as a function of temperature (only crystalline fractions are included).

T (K)	C	β-S	C$\underline{S}$	α-C_2S	α'_H-C_2S	$C_4A_3\underline{S}$	C_4AF
1053	62.5 (3)	25.4 (9)	12.2 (6)	–	–	–	–
1253	36.3 (6)	32.5 (9)	6.9 (8)	–	18.0 (9)	6.2 (8)	–
1343	–	2.4 (8)	–	9.4 (7)	36.0 (9)	41.8 (7)	10.3 (9)
1388	–	–	–	10.7 (7)	36.0 (9)	39.5 (7)	13.9 (9)
1423	–	–	–	11.1 (5)	39.1 (9)	32.8 (6)	16.9 (8)
1488	–	–	–	13.9 (6)	35.1 (9)	28.0 (5)	22.8 (8)
1553	–	–	–	23.1 (9)	46.9 (9)	30.0 (6)	–
1608	–	–	–	65.9 (5)		34.1 (9)	–
1648	–	–	–	71.9 (7)		28.1 (9)	–

Table 4
Direct Rietveld quantitative phase results (wt%) for Fe_BSA_B2 as a function of temperature (only crystalline fractions are included).

T (K)	C	β-S	C$\underline{S}$	α-C_2S	α'_H-C_2S	$C_4A_3\underline{S}$	C_4AF
913	62.2 (3)	26.2 (8)	11.6 (6)	–	–	–	–
1073	53.1 (3)	23.9 (7)	9.6 (5)	–	13.5 (9)	–	–
1128	52.5 (3)	25.3 (7)	10.8 (3)	–	11.5 (9)	–	–
1203	45.3 (3)	30.7 (7)	11.5 (5)	–	12.5 (9)	–	–
1253	24.6 (4)	17.4 (6)	4.8 (5)	6.8 (6)	25.7 (9)	17.2 (6)	3.5 (9)
1288	2.8 (3)	6.5 (5)	1.1 (2)	4.0 (5)	43.7 (9)	33.9 (6)	8.0 (8)
1373	–	–	–	5.3 (5)	48.2 (9)	31.8 (5)	14.7 (7)
1433	–	–	–	8.1 (5)	39.5 (9)	33.5 (5)	18.9 (7)
1513	–	–	–	45.5 (5)	2.5 (6)	39.2 (5)	12.8 (8)
1568	–	–	–	59.5 (9)	–	40.5 (5)	–
1613	–	–	–	72.1 (5)	–	27.9 (8)	–
1663	–	–	–	100 (–)	–	–	–

those from clinker ones were 2000 counts s^{-1}. Therefore, the diffraction signal of clinker phases is in the range 5–10% of the overall measured data. However, the good statistics from synchrotron radiation allows RQPA to be carried out.

Fe_BSA_B1 will be used to detail the most important results for the clinkering study of this family of materials. Firstly, at 1053 K, a large amount of phases arising from the decomposition of the raw materials, such as free lime (red stars), β-SiO_2 (black triangle) and anhydrite (green triangle), are quantified. Fig. 5(*a*) shows the Rietveld plot for Fe_BSA_B1 at 1053 K. Al_2O_3-rich amorphous content, composed of metakaolin (Siddique & Klaus, 2009) and γ-Al_2O_3, and ill-crystallized Fe_2O_3 is likely to be present at these low temperatures. As temperature increases, free lime reacts to form $C_4A_3\underline{S}$ (blue circles), α'_H-C_2S (purple squares) and C_4AF (red diamonds). Over 1388 K, free lime has reacted completely. It is noticeable that under these experimental conditions the undesirable C_2AS or $C_5S_2\underline{S}$ phases have not been detected at any temperature, which is a good result as these phases are non-hydraulic active (Li *et al.*, 2001). At 1488 K, Fig. 5(*b*), the phase assemblage determined by the Rietveld method [49 (1) wt% C_2S, 28 wt% $C_4A_3\underline{S}$ and 23% C_4AF; Table 3] is in very good agreement with the theoretical/expected composition [50 wt% C_2S, 30 wt% $C_4A_3\underline{S}$ and 20% C_4AF]. Therefore, the accuracy of this type of analysis is reasonably good. One possibility to further improve the accuracy is to have better signal-to-noise diffraction data by increasing the amount of clinker particles within the synchrotron beam. This could be achieved by using a Pt capillary with larger diameter and the same wall size. However, the mechanical stability under rotation at high temperatures has to be proven.

The optimum clinkering temperatures, which correspond to the largest overall amount of $C_4A_3\underline{S}$, were 1543 K for Fe_BSA_B0 (Table 2), 1488 K for Fe_BSA_B0 (Table 3) and 1433 K for Fe_BSA_B2 (Table 4). Thus, clinkering temperatures have been determined and it is proved that the addition of boron and sodium to raw materials decreases the maximum temperature needed to obtain the expected phase assemblage. Moreover, at these temperatures the highest quantities of crystalline $C_4A_3\underline{S}$ and C_4AF are formed, 28.0 (5) and 22.8 (8) wt%, respectively, for Fe_BSA_B1. These values are used to indirectly infer the amount of liquid phase or melting that is appearing using the following expression: $L = [(M_v - R_F)/(100 - R_F)] \times 100$, where L stands for the amount of liquid phase in wt%, M_v stands for the largest quantities of crystalline $C_4A_3\underline{S}$ and C_4AF, and R_F stands for the remaining phases that are partially melted at the given temperature. For example, for Fe_BSA_B1 at 1553 K, M_v was 50.8 and R_F was 30.0 wt%; consequently, L was calculated to be 29.7 wt%. This value of liquid phase is used to normalize direct Rietveld results at the given temperature. Above 1488 K the aluminium-rich phases, $C_4A_3\underline{S}$ and C_4AF, start to melt. Fig. 5(*c*) shows Fe_BSA_B1 at 1648 K where C_4AF is completely melted. Thus, RQPA results from patterns at higher temperatures have to be renormalized, since there is a liquid phase appearing. For instance, for Fe_BSA_B1 at 1648 K the renormalized analysis is 50.2 wt% of α-C_2S, 19.6 wt% of $C_4A_3\underline{S}$ and 30.2 wt% of melt phase. Fig. 6 shows normalized/renormalized RQPA results including the derived liquid phase content for Fe_BSA_B*x* clinkers at very high temperatures.

As the Pt capillary is fully bathed within the X-ray beam, the absolute (integrated) intensities provide useful information. The maximum amount of $C_4A_3\underline{S}$ in Fe_BSA_B1, Fig. 3, takes place at 1488 K. Above this temperature, Fig. 3 clearly shows that the absolute intensities of $C_4A_3\underline{S}$ diffraction peaks

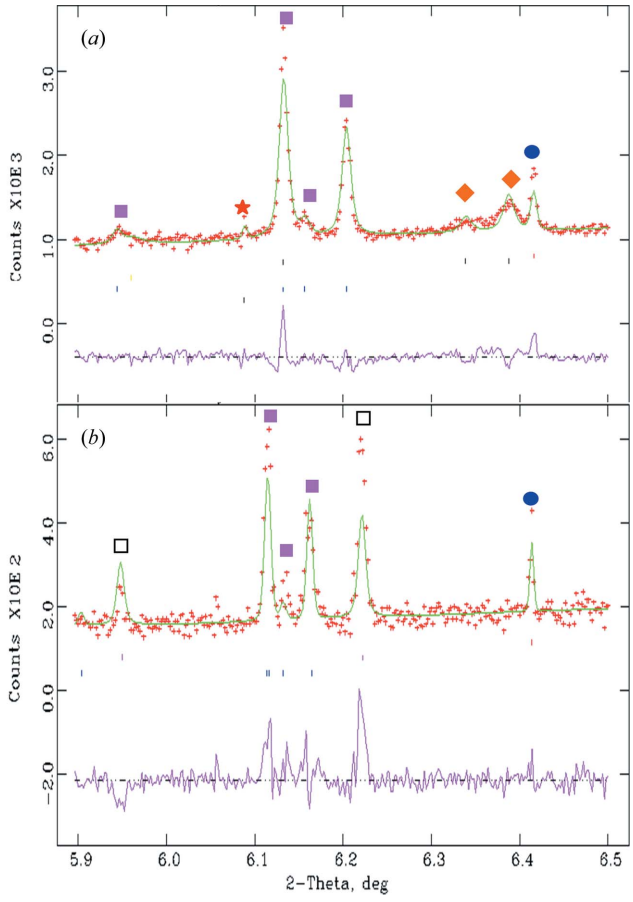

Figure 4
Enlarged range of Rietveld plots for (*a*) Fe_BSA_B0 at 1428 K and (*b*) Fe_BSA_B1 at 1553 K. Symbols are as in Figs. 1 and 3.

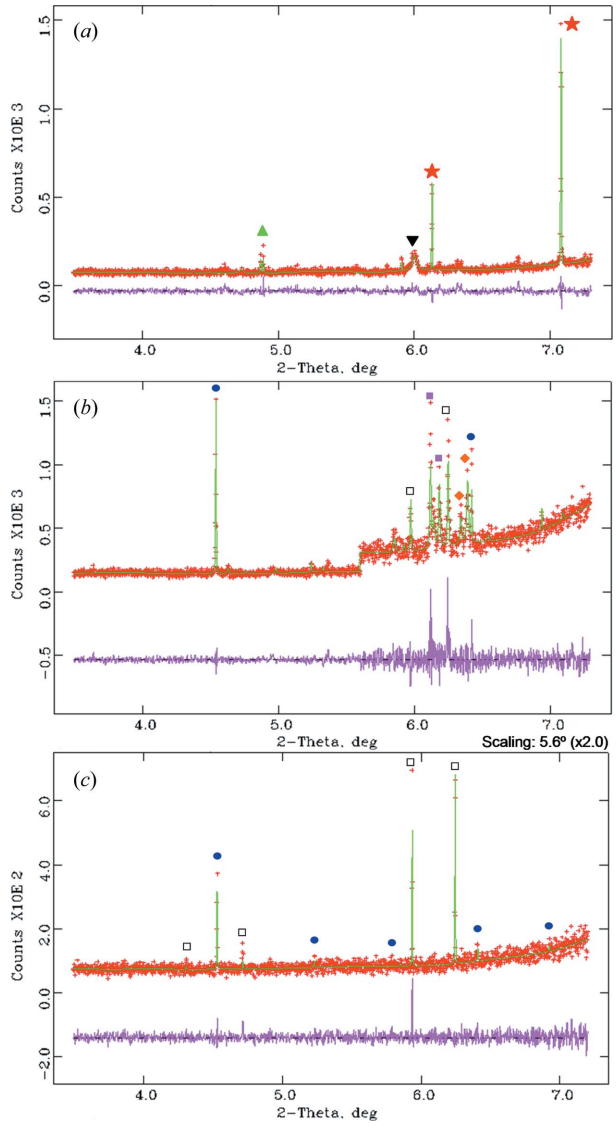

Figure 5
Rietveld plot for Fe_BSA_B1 at (*a*) 1053 K, (*b*) 1488 K and (*c*) 1648 K, where the symbols highlight the phases as in Fig. 3. In (*b*) the represented data from 5.6° 2θ have been multiplied by 2 in order to better show the peaks which have low intensities.

decrease. Thus, the overall amount of crystalline $C_4A_3\underline{S}$ decreases at 1553 K and it is strongly reduced at 1608 K. However, a diffraction experiment cannot distinguish between decomposition and melting of a given phase. However, according to the ATD_TG study (see below), this diminution is likely to be due to the decomposition of this phase. It is known that $C_4A_3\underline{S}$ incongruently decomposes at high temperature to yield calcium aluminates and $C\underline{S}$. These phases are not detected above ∼1550 K because aluminates are melted and $C\underline{S}$ is also decomposing at these temperatures. This decomposition is in agreement with a report by Puertas *et al.* (1995) that stated that $C_4A_3\underline{S}$ decomposes to yield $C_{12}A_7$ and SO_3 above approximately 1573 K after several hours of thermal treatment.

An important result reported in Tables 2–4 and Fig. 6 is the modification of the α'_H-C_2S to α-C_2S phase transition temperature with B/Na doping. For all the compositions the temperature of this transformation is lower than that published for pure C_2S, 1698 K (Taylor, 1997). Moreover, as the amount of B_2O_3/Na_2O increases, the phase transition temperature decreases. α-C_2S appears above 1633 K for Fe_BSA_B0, while 9.4 (7) wt% of this phase is quantified at 1343 K for Fe_BSA_B1 and 6.8 (6) wt% at 1253 K in Fe_BSA_B2.

Figs. 7(*a*), 7(*b*) and 7(*c*) show DTA-TG curves for Fe_BSA_B0, Fe_BSA_B1 and Fe_BSA_B2 raw materials, respectively. The overall shapes are quite similar but there are variations in the temperature of the different reactions/processes. Therefore, these thermal-activated processes will be discussed for the series. The first two small endothermic peaks, (1) and (2) (see Fig. 7), correspond to the dehydration of gypsum and dehydroxylation of kaolin, respectively. This association is due to the temperature of the processes and it is also in agreement with the measured associated weight losses. The strong endothermic effect at ∼1070 K, (3), with a huge associated weight loss, is due to the decomposition of $CaCO_3$. The temperature variation of these three processes along the series is negligible, as expected. Between ∼1150 K and ∼1450 K there is no weight loss and some minor thermal effects can be observed. In this temperature range the trans-

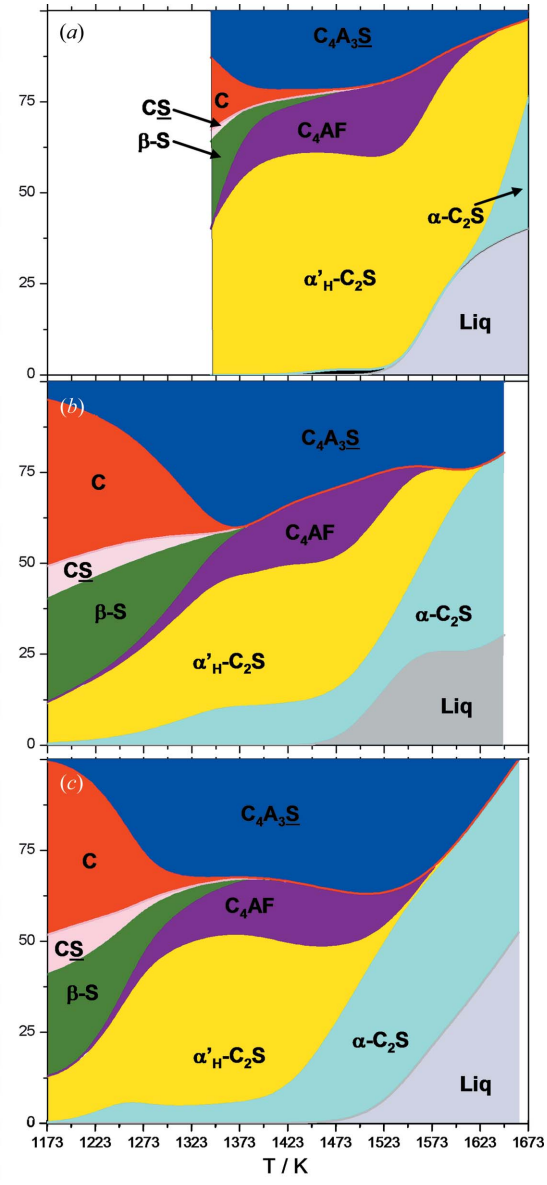

Figure 6
Normalized phase evolution with temperature for (*a*) Fe_BSA_B0, (*b*) Fe_BSA_B1 and (*c*) Fe_BSA_B2 clinkering.

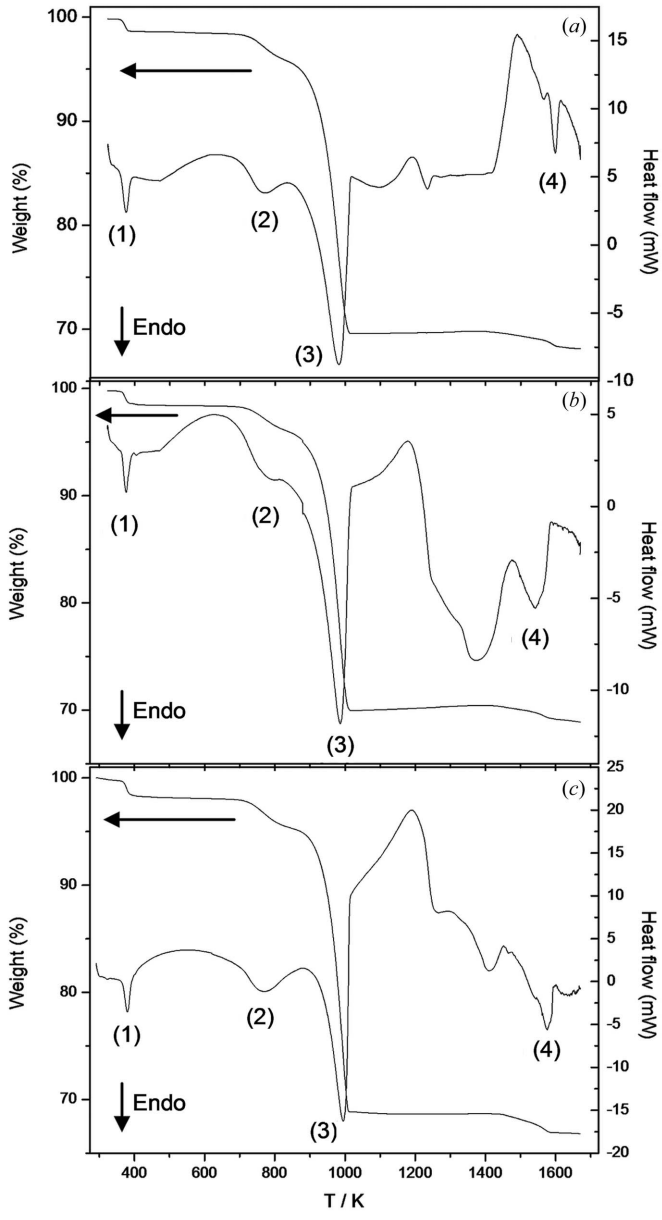

Figure 7
DTA-TGA curves for (*a*) Fe_BSA_B0, (*b*) Fe_BSA_B1 and (*c*) Fe_BSA_B2 raw mixtures.

formation of metakaolin into a spinel-like transient phase (Sanz *et al.*, 1991), the formation of $C_4A_3\underline{S}$ and the α'_H-$C_2S \rightarrow \alpha$-C_2S transformation take place. Finally, the last broad endotherm, (4), takes place at temperatures close to 1550 K and it is very likely related to partial decompositionof $C_4A_3\underline{S}$. This effect has associated weight losses of 1.7 wt%, 1.6 wt% and 1.9 wt% for Fe_BSA_B0, Fe_BSA_B1 and Fe_BSA_B2, respectively. This is in agreement with previous reports (Puertas *et al.*, 1995; Li *et al.*, 2007) dealing with thermal decomposition of $C_4A_3\underline{S}$ at very high temperatures. This observation is also in agreement with the powder diffraction result discussed above. It must be underlined that the measured weight losses do not correspond to full $C_4A_3\underline{S}$ decomposition with the consequent SO_3 release. The measured weight losses indicated the $C_4A_3\underline{S}$ decomposition ratio ranges 35–48%. Therefore, in the reported experimental conditions of the thermal study, only up to 50% of Klein's salt is decomposed at 1670 K.

3.3. *In situ* Al-rich BSA clinker formation

A similar *in situ* powder diffraction study has been performed for an Al-rich belite sulfoaluminate clinker. Table 5 gives direct RQPA results for the temperatures studied. Fig. 8 shows normalized quantitative phase results for all the temperatures, where liquid phase is included if necessary. As was the case for Fe-rich clinkers, phases related to raw materials (free lime, anhydrite and β-SiO_2) still remain at 1293 K. At this temperature small amounts of α'_H-C_2S, CA and $C_4A_3\underline{S}$ are being formed. As temperature increases raw materials are reacting and the amounts of the later phases

Table 5
Direct Rietveld quantitative phase analysis results (wt%) for Al_BSA as a function of temperature (only crystalline fractions are included).

T (K)	C	C$\underline{S}$	b-S	α'_H-C_2S	CA	C_3A	$C_{12}A_7$	$C_4A_3\underline{S}$
1213	47.0 (2)	7.2 (5)	24.8 (6)	18.8 (6)	–	–	–	2.2 (4)
1293	19.6 (2)	2.7 (3)	14.4 (4)	42.2 (5)	5.1 (6)	–	–	15.9 (3)
1323	8.6 (2)	–	2.2 (2)	54.7 (3)	3.9 (5)	–	2.3 (2)	28.4 (3)
1368	5.9 (1)	–	1.8 (2)	58.5 (3)	5.3 (5)	1.5 (2)	6.0 (2)	20.9 (2)
1403	3.2 (1)	–	1.1 (1)	55.7 (3)	5.9 (5)	2.3 (2)	8.1 (2)	23.6 (2)
1448	1.4 (1)	–	–	53.8 (3)	5.6 (5)	5.4 (2)	11.1 (2)	22.7 (2)
1538	–	–	–	51.8 (2)	5.7 (4)	7.0 (2)	13.9 (2)	21.7 (2)
1583	–		–	53.1 (2)	5.6 (4)	5.2 (2)	16.8 (2)	19.1 (2)
1623	–	–	–	71.3 (2)	–	–	4.2 (2)	24.5 (2)
1643	–	–	–	76.5 (2)	–	–	–	23.5 (3)

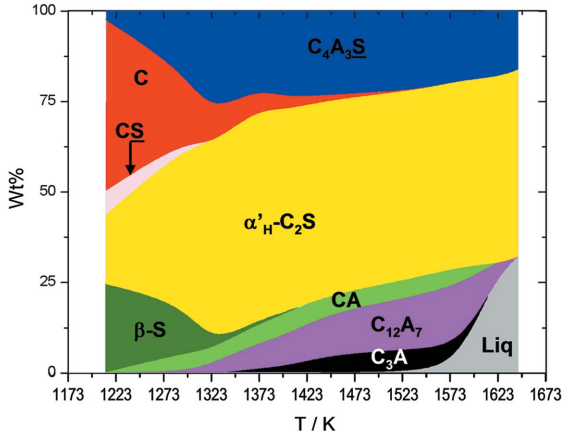

Figure 8
Normalized phase evolution with temperature for Al_BSA clinkering.

increase. Furthermore, $C_{12}A_7$ and C_3A phases appear. At 1538 K the maximum content of crystalline phases, including $C_4A_3\underline{S}$, is obtained, so this is the optimum clinkering temperature. At higher temperatures, aluminium-rich phases start to melt. At 1583 K, the $C_{12}A_7$/CA ratio is 3. This composition corresponds to a eutectic point in the binary system at 1663 K (Chatterjee & Zhmoidin, 1972). In the studied quaternary system the melted phase appears at a lower temperature, as expected. At 1623 K, C_3A and CA are fully melted; meanwhile $C_{12}A_7$ is only partially melted. It is noticeable that $C_4A_3\underline{S}$, for this clinker composition, decomposes at a lower pace (higher temperatures) than for related Fe-rich compositions. The weight loss owing to SO_3 release (arising from $C_4A_3\underline{S}$ decomposition) was reported to be 1.0 wt% (Martín-Sedeño *et al.*, 2010), which is lower than those obtained here for Fe-rich compositions (see above). On the other hand, it must also be highlighted that for this Al-rich composition the α'_H-C_2S → α-C_2S polymorphic transformation does not take place in the studied temperature range.

3.4. Minor elements effects: unit-cell values and temperature transformations

Boron oxide and sodium oxide have been added to iron-rich raw mixtures in order to promote the stabilization at room temperature of the high-temperature α-forms of C_2S (Cuberos *et al.*, 2010). In this study it has been proved that the α'_H-C_2S → α-C_2S polymorphic transformation temperature decreases as minor element contents increase. Figs. 9(*a*) and 9(*b*) report refined unit-cell volumes (V/Z) for α-C_2S and α'_H-C_2S, respectively. Bibliographic data (Remy & Andrault, 1997) of unit-cell volume variation for pure C_2S have been included for the sake of comparison as black solid lines. It is proved that the transformation temperature for C_2S polymorphs has been decreased by addition of B_2O_3 and Na_2O in agreement with previous results (Fukuda *et al.*, 2001). The unit-cell volumes of dicalcium silicate in Al_BSA, Fe_BSA_B0 and Fe_BSA_B1 are larger than those of pure C_2S at the same temperature, as expected owing to the dopant

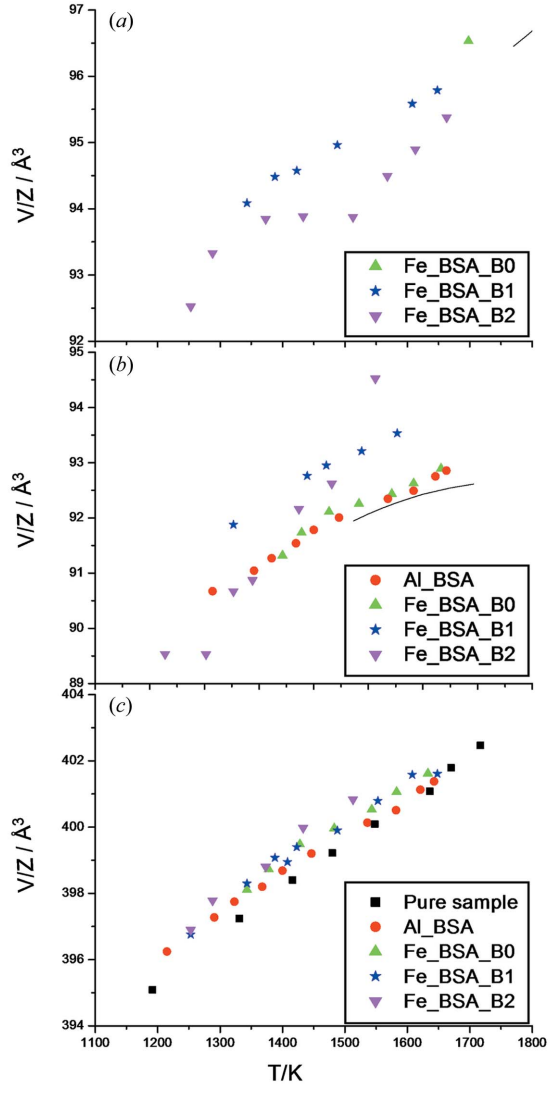

Figure 9
Variation of refined unit-cell volumes (V/Z) as a function of temperature for (*a*) α-C_2S, (*b*) α'_H-C_2S and (*c*) $C_4A_3\underline{S}$. Data from samples are plotted. Data from pure C_2S taken from Remy & Andrault (1997) are shown as black solid lines.

incorporation. However, the α-C_2S and α'_H-C_2S unit-cell volumes in Fe_BSA_B2 are smaller than expected. Research on C_2S solid solutions with B_2O_3 and Na_2O is in progress in order to understand the stabilization mechanism by partial elemental substitution with possible vacancy incorporation within the crystal structures.

Fig. 9(*c*) reports refined unit-cell volumes (V/Z) for the $C_4A_3\underline{S}$ phase in all studied samples, as a function of temperature. The variation of unit-cell volume is linear for all compositions. This figure includes data of the pure phase $C_4A_3\underline{S}$ unit-cell expansion (De la Torre *et al.*, 2011). $C_4A_3\underline{S}$ for all clinker compositions have unit-cell volumes larger than that of the pure phase. The volumes of $C_4A_3\underline{S}$ for Fe-rich compositions increase as the amounts of B_2O_3 and Na_2O increase, as expected. On the other hand, and as discussed above, the temperature of the decomposition/melting of $C_4A_3\underline{S}$ slightly decreases with the addition of the activators.

4. Conclusions

Clinkering reactions of belite sulfoaluminate clinkers have been studied *in situ*. Several reactions have been followed including the α'_H-$C_2S \rightarrow \alpha$-C_2S polymorphic transformation, the decomposition of $C_4A_3\underline{S}$ and the melting of C_4AF. Overall, these temperatures decrease as the added amount of B_2O_3 and Na_2O increases. For instance, the $\alpha'_H \rightarrow \alpha$ polymorphic transformation takes place at $\sim$1650 K in the reference clinker and it is lowered at $\sim$1350 and 1250 K for clinkers with 1 wt% and 2 wt% B_2O_3, respectively. The decomposition temperature of $C_4A_3\underline{S}$ is also lowered from $\sim$1550 K in the reference clinker to $\sim$1500 K in the clinker with the largest amount of added borax. Furthermore, this addition also decreases the melting temperatures of C_4AF from $\sim$1550 K to $\sim$1430 K. Finally, optimum clinkering temperatures decrease with borax addition and they have been determined as being $\sim$1490 and $\sim$1430 K for Fe_BSA_B1 and Fe_BSA_B2 clinkers, respectively.

Financial support from MAT2010-16213 research grant (MICINN, Spain) is acknowledged. ESRF is thanked for the provision of synchrotron X-ray beam time at ID31 beamline.

References

Adolfsson, D., Menad, N., Viggh, E. & Bjorkman, B. (2007). *Adv. Cem. Res.* **19**, 133–138.

Arblaster, J. W. (2006). *Platinum Metals Rev.* **50**, 118–119.

Arjunan, P., Silsbee, M. R. & Roy, D. M. (1999). *Cem. Concr. Res.* **29**, 1305–1311.

Beretka, J., Marroccoli, M., Sherman, N. & Valenti, G. L. (1996). *Cem. Concr. Res.* **26**, 1673–1681.

Chatterjee, A. K. & Zhmoidin, G. I. (1972). *J. Mater. Sci.* **7**, 93–97.

Christensen, A. N., Scarlett, N. V. Y., Madsen, I. C., Jensen, T. R. & Hanson, J. C. (2003). *J. Chem. Soc. Dalton Trans.* **8**, 1529–1536.

Chung, D. D. L., DeHaven, P. W., Arnold, H. & Ghosh, D. (1993). *X-ray Diffraction at Elevated Temperatures.* New York: VCH.

Cuberos, A. J. M., De la Torre, A. G., Álvarez-Pinazo, G., Martín-Sedeño, M. C., Schollbach, K., Pöllmann, H. & Aranda, M. A. G. (2010). *Environ. Sci. Technol.* **44**, 6855–6862.

Cuberos, A. J. M., De la Torre, A. G., Martín-Sedeño, M. C., Moreno-Leal, L., Merlini, M., Ordonez, L. M. & Aranda, M. A. G. (2009). *Cem. Concr. Res.* **39**, 833–842.

De la Torre, A. G. & Aranda, M. A. G. (2003). *J. Appl. Cryst.* **36**, 1169–1176.

De la Torre, A. G., Cabeza, A., Calvente, A., Bruque, S. & Aranda, M. A. G. (2001). *Anal. Chem.* **73**, 151–156.

De la Torre, A. G., Cuberos, A. J. M., Alvarez-Pinazo, G., Cuesta, A. & Aranda, M. A. G. (2011). *Proceedings of 13th International Congress on the Chemistry of Cements*, Madrid, Spain. In the press.

De la Torre, A. G., Morsli, K., Zahir, M. & Aranda, M. A. G. (2007). *J. Appl. Cryst.* **40**, 999–1007.

Finger, L. W., Cox, D. E. & Jephcoat, A. P. (1994). *J. Appl. Cryst.* **27**, 892–900.

Fiquet, G., Richet, P. & Montagnac, G. (1999). *Phys. Chem. Miner.* **27**, 103–111.

Fukuda, K., Takeda, A. & Yoshida, H. (2001). *Cem. Concr. Res.* **31**, 1185–1189.

Gartner, E. (2004). *Cem. Concr. Res.* **34**, 1489–1498.

Glasser, F. P. & Zhang, L. (2001). *Cem. Concr. Res.* **31**, 1881–1886.

Grain, C. F. & Campbell, W. J. (1962). *US Bur. Mines Rep. Invest.* **5982**, 21.

Gualtieri, A. F., Lassinantti Gualtieri, M. & Meneghini, C. (2008). *Powder Diffr.* **23**, 323–328.

Janotka, I., Krajèi, L. & Mojumdar, S. C. (2007). *Ceram. Silic.* **51**, 74–81.

Larson, A. C. & Von Dreele, R. B. (1994). Los Alamos National Laboratory Report LA-UR-86, p. 784. Los Alamos National Laboratory, NM, USA.

León-Reina, L., De la Torre, A. G., Porras-Vázquez, J. M., Cruz, M., Ordonez, L. M., Alcobé, X., Gispert-Guirado, F., Larrañaga-Varga, A., Paul, M., Fuellmann, T., Schmidt, R. & Aranda, M. A. G. (2009). *J. Appl. Cryst.* **42**, 906–916.

Li, G. S. & Gartner, E. M. (2006). French patent application 04–51586 (publication 2873366).

Li, H., Agrawal, D. K., Cheng, J. & Silsbee, M. R. (2001). *Cem. Concr. Res.* **31**, 1257–1261.

Li, Y., Liu, X., Niu, X. & Song, L. (2007). *Mater. Res. Innov.* **11**, 92–94.

Madsen, I. C., Scarlett, N. V. Y., Cranswick, L. M. D. & Lwin, T. (2001). *J. Appl. Cryst.* **34**, 409–426.

Marchi, M., Costa, U. & Artioli, G. (2007). *Proceedings of the 12th International Congress on the Chemistry of Cements*, Montreal, Canada. W2-06.1.

Martín-Sedeño, M. C., Cuberos, A. J. M., De la Torre, A. G., Álvarez-Pinazo, G., Ordóñez, L. M., Gateshki, M. & Aranda, M. A. G. (2010). *Cem. Concr. Res.* **40**, 259–269.

Merlini, M., Artioli, G., Cerulli, T., Cella, F. & Bravo, A. (2008). *Cem. Concr. Res.* **38**, 477–486.

Morsli, K., De la Torre, A. G., Stöber, S., Cuberos, A. J. M., Zahir, M. & Aranda, M. A. G. (2007*a*). *J. Am. Ceram. Soc.* **90**, 3205–3212.

Morsli, K., De la Torre, A. G., Zahir, M. & Aranda, M. A. G. (2007*b*). *Cem. Concr. Res.* **37**, 639–646.

Moussa, S. M., Ibberson, R. M., Bieringer, M., Fitch, A. N. & Rosseinsky, M. J. (2003). *Chem. Mater.* **15**, 2527–2533.

Pera, J. & Ambroize, J. (2004). *Cem. Concr. Res.* **34**, 671–676.

Peterson, V. K., Ray, A. & Hunter, B. A. (2006). *Powder Diffr.* **21**, 12–18.

Phair, J. W. (2006). *Green Chem.* **8**, 763–780.

Popescu, C. D., Muntean, M. & Sharp, J. H. (2003). *Cem. Concr. Composites*, **25**, 689–693.

Puertas, F., Blanco-Varela, M. T. & Giménez-Molina, S. (1995). *Cem. Concr. Res.* **25**, 572–580.

Quillin, K. (2001). *Cem. Concr. Res.* **31**, 1341–1349.

Remy, C. & Andrault, D. (1997). *J. Am. Ceram. Soc.* **80**, 851–860.

Sanz, J., Sobrados, I., Cavalieri, A. L., Pena, P., De Aza, S. & Moya, J. S. (1991). *J. Am. Ceram. Soc.* **74**, 2398–2403.

Scarlett, N. V. Y., Madsen, I. C., Cranswick, L. M. D., Lwin, T., Groleau, E., Stephenson, G., Aylmore, M. & Agron-Olshina, N. (2002). *J. Appl. Cryst.* **35**, 383–400.
Selcuk, N., Soner, I. & Selcuk, E. (2010). *Adv. Cem. Res.* **22**, 107–113.
Siddique, R. & Klaus, J. (2009). *Appl. Clay Sci.* **43**, 392–400.
Taylor, H. F. W. (1997). *Cement Chemistry*. London: Thomas Telford.
Thompson, P., Cox, D. E. & Hastings, J. B. (1987). *J. Appl. Cryst.* **20**, 79–83.
Toby, B. H. (2001). *J. Appl. Cryst.* **34**, 210–213.
Winnefeld, F. & Barlag, S. (2009). *ZKG Intl.* **12**, 42–53.